

The Circumstellar Envelope of π^1 Gru

G.R. Knapp¹, and K. Young² and M. Crosas²

¹ Department of Astrophysical Sciences, Princeton University, Princeton, NJ 08544, USA; gk@astro.princeton.edu

² Harvard-Smithsonian Center for Astrophysics, 60 Garden St., Cambridge, MA 02138, USA; rtm@dolson.harvard.edu, mcrosas@cfa.harvard.edu

Abstract. CO(J = 2–1) and SiO(J = 5–4) emission has been observed from the molecular envelope around the nearby S star π^1 Gru. The CO line profile differs from the usual parabolic shape seen in uniformly-expanding envelopes; it has a Voigt-like profile and two horns. A model for line formation in the envelope shows that a tilted, expanding disk reproduces the observations well. The star also has a fast molecular wind, with a projected outflow speed of at least 70 and perhaps as high as 90 km s⁻¹. The fast wind is presumably ejected from the poles of the disk. These observations show that the complex structure seen in many planetary nebulae, including quadrupolar structure and fast winds, may largely evolve from structure formed while the progenitor star is in the last stages of evolution on the AGB.

Key words: radio lines: stars — stars: AGB and post-AGB — stars: mass loss — stars: S stars

1. Introduction

Mass loss from stars on the Asymptotic Giant Branch (AGB) takes place as a cool, dusty, molecular wind at rates which are so high that they dominate the evolution of the star. The energy in these huge stars is produced in their very small cores, leading to the expectation that the structure of the star and of its circumstellar outflow will be spherically symmetric. However, a plethora of recent observations (e.g. Lucas 1999; Monnier 1999; Tuthill et al. 1999; Monnier et al. 1999) have shown that the outflows are far from smooth, steady, uniform and spherically symmetric, and that asymmetries can be seen on a wide range of size scales. This paper discusses molecular line observations of the envelope of π^1 Gru, which is known to have complex structure and large-scale asymmetry from previous CO observations (Sahai 1992, hereafter S92).

π^1 Gru is a nearby mass-losing S star, at a distance of 153 pc (Perryman et al. 1997; van Eck et al. 1998). S92 found that the CO line profiles have a very unusual shape: they are double-horned, and do not have the steep sides typical of molecular line emission from uniformly expand-

ing stellar winds. Further, the envelope has north-south kinematic structure, and at least two velocity components; a “normal” outflow with an apparent speed of about 11 km s⁻¹, and a faster outflow with a speed of ≥ 38 km s⁻¹.

The molecular line observations measure a mean mass loss rate of several $\times 10^{-7} M_{\odot}$ yr⁻¹, while the 60 μ m emission from circumstellar dust shows that the envelope is extended (Young et al. 1993), with a radius of about 6×10^{17} cm and a kinematic age of $\sim 10^4$ years. π^1 Gru is the primary of a wide binary system, whose secondary, at a projected separation of 2.7'', appears to be a solar-mass main sequence star (Proust et al. 1981; Ake & Johnston 1992). The stars are thus at least 6×10^{15} cm apart and, since the system mass is at least $2 M_{\odot}$, the orbital period is about 6000 years and the orbital velocity about 2 km s⁻¹.

Given the possible presence of a fast molecular wind and bipolar structure in the envelope of π^1 Gru, plus the presence of its binary companion, we reobserved the envelope with improved sensitivity and modeled its line emission in an attempt to better define its geometry and kinematics. These observations are described in the next section, and the results are given in Section 3. Section 4 describes a model of the structure of the circumstellar envelope. These results are discussed in Section 5, and Section 6 contains the conclusions.

2. Observations

The properties of π^1 Gru from the literature, plus those derived in the present paper, are summarized in Table 1. The distance is from the Hipparcos parallax (Perryman et al. 1997), the luminosity from van Eck et al. (1998), and the variability type and period from Proust et al. (1981), and Kerschbaum & Hron (1994).

The observations were made with the 10.4m Robert B. Leighton telescope of the Caltech Submillimeter Observatory on Mauna Kea, Hawai'i, on September 4-6 1997. The southerly declination of the star means that it is always at a low zenith angle as observed from the CSO, and the consequent high air mass makes submillimeter observations, which have higher angular resolution, impractical. The star was observed in the relatively transparent 1.2

Table 1. Observed Properties of π^1 Gru

$\alpha(1950)$	22 ^h 19 ^m 41.13 ^s
$\delta(1950)$	-46° 12' 02.4''
Spectral Type	S5.7
Variable Type	SRb
Period	150 ^d
Distance	153 +28, -20 pc
L_{bol}	7450 L_{\odot}
SiO(6-5):	
I	$0.75 \pm 0.05 \text{ K} \times \text{km s}^{-1}$
T_{MB}	$0.042 \pm 0.005 \text{ K}$
V_{o}	$13.1 \pm 2.1 \text{ km s}^{-1}$
V_{c}	$-12.6 \pm 0.8 \text{ km s}^{-1}$
CO(2-1) (high resolution):	
Projected V_{o}	5.1 km s^{-1}
V_{c}	-11.8 km s^{-1}
Mean \dot{M}	$4.5 \times 10^{-7} M_{\odot} \text{ yr}^{-1}$
CO(2-1) (map):	
Projected V_{o}	6.4 km s^{-1}
V_{c}	-11.7 km s^{-1}
\dot{M}	$1.2 \times 10^{-6} M_{\odot} \text{ yr}^{-1}$
V_{o}	15 - 18 km s^{-1}

mm window, in the CO(2-1) line at 230.538 GHz and the SiO(6-5) line at 260.518 GHz. The telescope half-power beamwidth was measured to be 30'', and the main beam efficiency to be 69%, using observations of Jupiter. The zenith atmospheric opacity τ_{o} was ~ 0.06 .

The observations used a liquid helium cooled SIS junction receiver with a double sideband system temperature of ~ 100 K. The temperature scale and the atmospheric opacity were measured by comparison with a room temperature load. The temperature scale was corrected for the atmospheric opacity and for the main beam efficiency.

The spectral lines were observed using two acousto-optic spectrographs with bandwidths of 500 MHz and 50 MHz respectively over 1024 channels. The spectrometer frequency, frequency scale and spectral resolution were calibrated using an internally generated frequency comb, and the velocity scale was corrected to the Local Standard of Rest (LSR). The velocity resolutions of the spectrometers were $\sim 2.1 \text{ km s}^{-1}$ and $\sim 0.21 \text{ km s}^{-1}$.

The observations were made by chopping between the star position and an adjacent sky position with the secondary mirror, using a chop throw of 120'' in azimuth at a rate of 1 Hz. Pairs of chopped observations were made with the star placed alternately in each beam. The spectral baselines resulting from this procedure are linear to within the r.m.s. noise for both spectrometers.

We performed three observations of the π^1 Gru envelope. First, we obtained a sensitive observation of the

CO(2-1) line with both the 50 MHz (high resolution) and 500 MHz (large bandwidth) spectrometers. The high resolution observation was made to measure the detailed shape of the strong CO line emission close to the systemic velocity of the star, while the large bandwidth observation was made to measure the weak emission from the star's high velocity molecular outflows. During these observations, the telescope pointing was checked roughly once per hour using the strong line emission. Second, we observed the SiO(6-5) line; because this line requires high density for excitation, and because much of the Si condenses onto dust close to the star, this emission arises from the inner regions of the envelope.

The third observation was a map of the CO(2-1) emission from the envelope made on a $100'' \times 100''$ square grid centered on the star's position and sampled every 10''. The observation was made using the 'on-the-fly' (OTF) technique. This method consists of scanning across the object's position and accumulating spectra as the telescope moves. The grid is built up by a set of scans stepped in the orthogonal direction. The map of π^1 Gru was made by executing several rapid complete OTF maps and summing them; this procedure minimizes errors due to pointing drifts. The OTF observations were made with the 500 MHz spectrometer only. Before each OTF map, the pointing was updated using the CO(2-1) line emission.

3. Results

The individual observations of the SiO(6-5) line were examined for bad baselines, co-added, and multiplied by the main beam efficiency. The resulting total SiO(6-5) line profile is shown in Fig. 1 (where it is compared with the high resolution CO(2-1) line profile, see below). The observed properties: the integrated intensity in $\text{K} \times \text{km s}^{-1}$; the peak line temperature; the wind outflow speed V_{o} ; and the central velocity V_{c} , are listed in Table 1. The central velocity and outflow velocity are in good agreement with the values found by S92 for the $^{13}\text{CO}(1-0)$ line. The SiO(6-5) line, like the $^{13}\text{CO}(1-0)$ line observed by S92, is roughly parabolic in shape, although the signal-to-noise ratio is not sufficient to definitively rule out a more complicated shape, such as the presence of horns. The profile does, however, show that the outflow velocity of the dense gas in the inner envelope is about 13 km s^{-1} .

Fig. 1 also shows the high resolution CO(2-1) line profile. The shape of this line is quite different from that of the SiO(6-5) line profile: it has two horns and a non-parabolic Voigt profile shape with a larger velocity extent. The mean velocity of the horns is -11.8 km s^{-1} , in good agreement with the central velocity of the SiO(6-5) and $^{13}\text{CO}(1-0)$ lines. The horns are offset in velocity from the line center by $\pm 5.1 \text{ km s}^{-1}$, about half the outflow velocity given by the SiO(6-5) line.

Fig. 2 shows the broad-band CO(2-1) line profile. High velocity molecular line emission is seen, extending

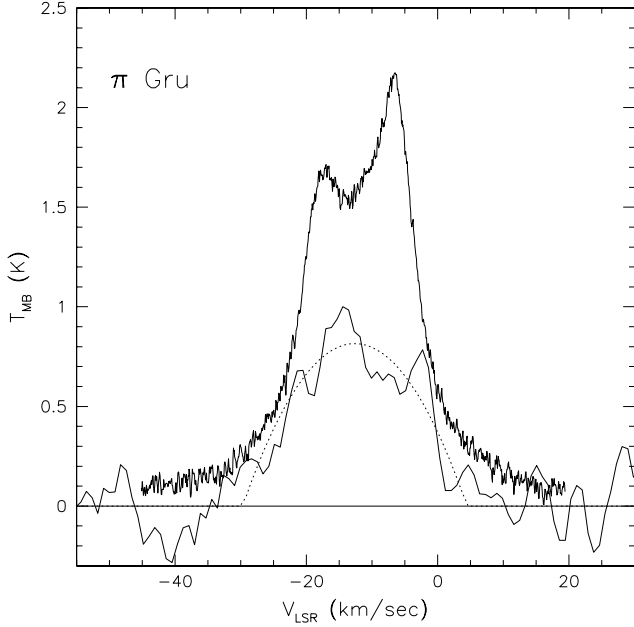


Fig. 1. CO(2–1) and SiO(6–5) line profiles from the circumstellar envelope of π^1 Gru. Dark line: CO(2–1) line profile observed at a resolution of 0.2 km s^{-1} . Light line: SiO(6–5) line observed at a resolution of 2 km s^{-1} . Dotted line: least-squares parabolic fit to the SiO(6–5) line profile. The temperature scale of the SiO(6–5) line has been multiplied by 20.

from about -100 km s^{-1} to at least $+40 \text{ km s}^{-1}$, and perhaps to $+80 \text{ km s}^{-1}$. This velocity range corresponds to -88 km s^{-1} to $+52 \text{ km s}^{-1}$ or $+92 \text{ km s}^{-1}$ with respect to the central velocity. The total extent of $140 - 180 \text{ km s}^{-1}$ is twice that seen in the lower signal to noise ratio observations of S92, and is almost certainly a lower limit to the true velocity extent of the fast wind.

Fig. 3 shows the CO(2–1) line profiles in a region $\pm 50''$ with respect to the star’s position. The emission is only slightly resolved by the $30''$ beam, but kinematic structure is clearly seen. This structure was examined by constructing a set of 11×11 pixel ($10''$ spacing) channel maps, i.e. maps of the emission at each velocity. The position of the emission peak in each map was measured using the routine IMFIT from the National Radio Astronomy Observatory’s AIPS data reduction package to fit a two-dimensional elliptical gaussian model. The results are shown in Fig. 4, which shows the declination and right ascension of the emission peak at each velocity. Near the systemic velocity, where the emission is strong, the data are plotted for every channel. At higher relative velocities, the data are averaged over 10 - 15 velocity channels. Also indicated in Figure 4 are the velocities of the emission horns determined from the central profile (Fig. 1) and the velocity range ($V_c \pm V_o$) of the SiO emission (Fig. 1).

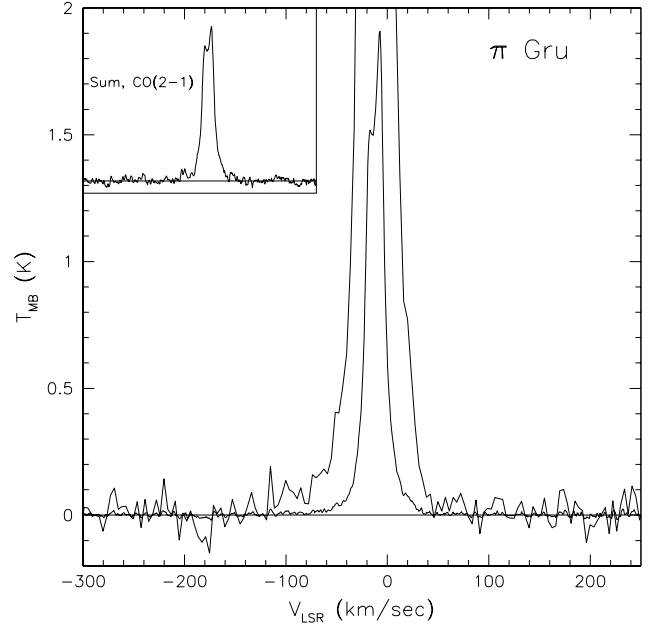


Fig. 2. CO(2–1) line profile of π^1 Gru (heavy line). Light line: scale increased by a factor of 10. The expanded profile has also been binned to a resolution of 4 km s^{-1} . Insert: the average CO(2–1) line profile from mapping observations over $\pm 30''$ about the star’s position (see Fig. 3). This profile is plotted on a velocity range of -200 to $+150 \text{ km s}^{-1}$.

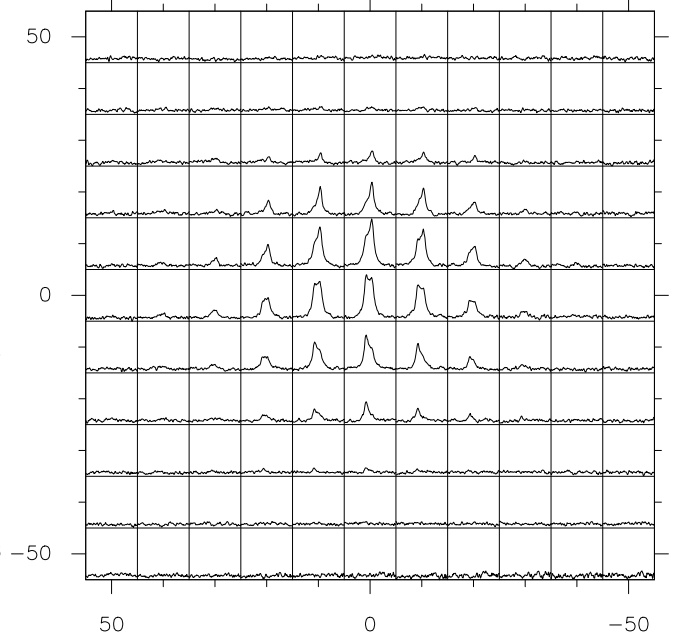


Fig. 3. RA-declination map of the CO(2–1) emission from π^1 Gru. The offsets are in arcseconds with respect to $\alpha(1950) = 22^{\text{h}} 19^{\text{m}} 41.13^{\text{s}}$, $\delta(1950) = -46^{\circ} 12' 02.4''$. The temperature scale for each profile runs from -0.2 to 2 K and the velocity scale from -100 to $+80 \text{ km s}^{-1}$.

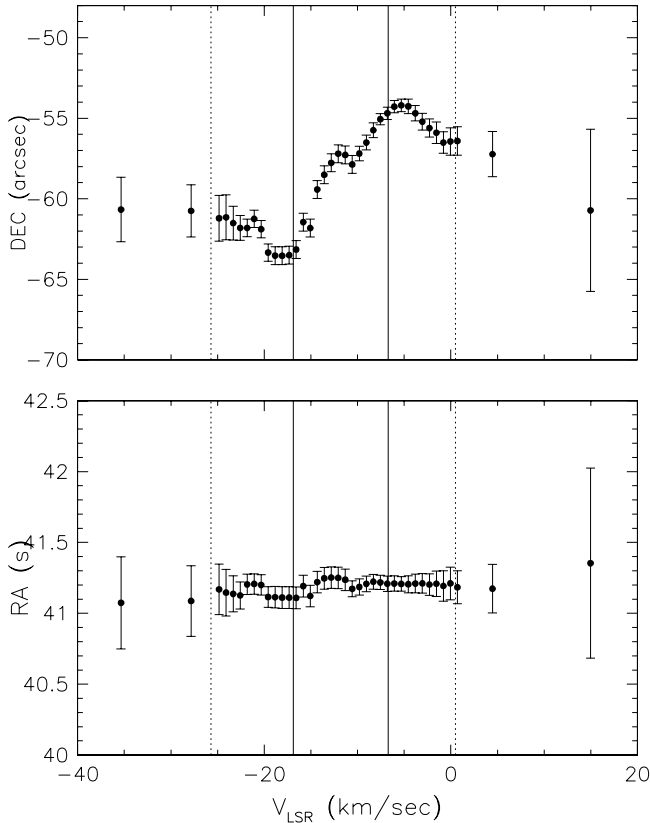


Fig. 4. Dependence of the position of peak CO(2–1) emission on velocity (a) upper panel: dependence on declination. The ordinate is arcseconds with respect to $\delta_o = -45^\circ 11' 00''$. The error bars are 1σ . The vertical solid lines show the velocities of the horns on the CO(2–1) line observed at the star’s position (Fig. 1). The vertical dotted lines show the velocity extent of the SiO(6–5) emission. (b) lower panel. As (a), for right ascension. The ordinate is with respect to $\alpha_o = 22^{\text{h}}19^{\text{m}}00^{\text{s}}$.

Fig. 4 reveals no resolvable kinematic structure in the EW direction, but shows velocity gradients in the NS direction, in agreement with S92. Fig. 4 shows that the two horns on the CO(2–1) line profile arise from different locations in the sky, separated by about $10''$.

At higher velocities with respect to the line center, $\pm(6$ to $12)$ km s^{-1} , the declination - velocity curve turns over. At higher velocities yet, the position offsets are smaller still and decrease essentially to zero. There is a second, lower amplitude inflection point in the velocity - right ascension curve near the central velocity, with a velocity gradient of ~ 5 km s^{-1} over a region a few arcseconds in diameter.

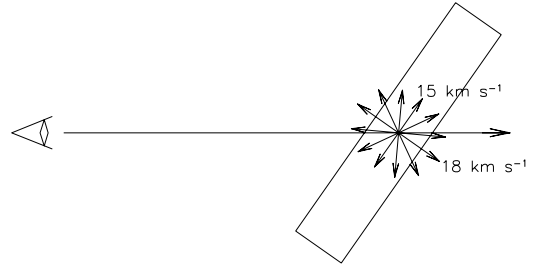


Fig. 5. Proposed model of the π^1 Gru circumstellar shell. The thickness of the model disk is one-fifth of its radius. The disk is inclined at 55° to the line of sight. North is up in this figure, east-west is perpendicular to the plane of the page. This model does not include the fast wind (see text)

4. A Model of the π^1 Gru Envelope

First we use a simple model for the molecular envelope to estimate an approximate mass loss rate. The SiO(6–5) line profile suggests simple spherical outflow, and we calculated a model CO emission profile assuming spherical outflow at constant velocity and mass loss rate, with a relative abundance $f = \text{CO}/\text{H}_2 = 6.5 \times 10^{-4}$ (Lambert et al. 1986), $V_o = 10$ km s^{-1} , and $\dot{M} = 4.5 \times 10^{-7} M_\odot \text{ yr}^{-1}$. The model CO(2–1) line profile is parabolic and does not reproduce the observed line shape.

We then investigated a model consisting of an expanding flattened system, or disk, tilted to the line of sight. The line profiles produced by this configuration were calculated from a model of the envelope geometry, with the line formation calculated by a Monte Carlo radiative transfer code based on that of Bernes (1979) modified for axisymmetric geometries. The envelope is modeled by a set of concentric rings, with sufficiently fine radial spacing to approximate a smooth distribution in optical depth (see Crosas & Menten 1997). The rings have 30 radial and 30 height spacings. Within each of the 30×30 rings, the density and temperature are constant. The 3D components of the velocity vector are calculated at each photon step (cf. Bernes 1979). The level populations are solved for 30 rotational levels and for infrared pumping to the first vibrational state ($v = 0 \rightarrow 1$ at $4.6 \mu\text{m}$) using the observed $4.6 \mu\text{m}$ flux density of π^1 Gru (Gezari et al. 1993). The mass loss rate, radial expansion velocity, turbulent velocity, kinetic temperature distribution and disk radius are input parameters. The line profile along a given line of sight is calculated by rotating the structure, calculating the line emission across the structure and convolving the emission with a two-dimensional circular gaussian beam. The fast molecular wind was not included in this model.

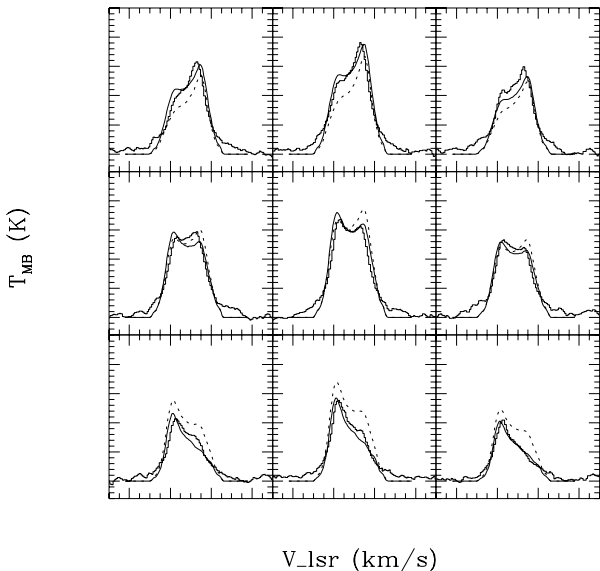


Fig. 6. Comparison of observed and model CO(2–1) line profiles for the envelope of π^1 Gru. The geometry of the model is shown in Fig. 6 and described in the text, and the calculated line profiles are compared with the data for the inner $20''$ of the envelope (cf. Fig. 3). The solid line shows the best fit model, which includes a pointing offset of $+5''$ in declination. The dashed lines show the calculated line profile assuming that the map is centered on the center of the envelope (see text).

A model in which the bulk of the CO(2–1) emission arises from a tilted, expanding disk produced by constant mass loss fits the data well. This model is sketched in Fig. 5 and the model and observed line profiles are compared in Fig. 6. The northern part of the disk is tilted away from the observer at an angle of 55° to the line of sight. The temperature profile is approximated as a power law: $T(r) = 300 \text{ K } (r/10^{15} \text{ cm})^{-0.7}$, as found in detailed models of AGB star winds (Goldreich & Scoville (1976); Kwan & Linke (1982)).

The best fit model has a disk radius of 5×10^{16} cm, a thickness of 10^{16} cm, and is produced by a constant mass loss rate of $1.2 \times 10^{-6} M_\odot \text{ yr}^{-1}$. The radial expansion velocity in the plane of the disk is 15 km s^{-1} , increasing slightly to 18 km s^{-1} at the poles, and the turbulent velocity is 1 km s^{-1} . It was also found that better agreement with the data is obtained if the telescope pointing is offset from the center of the envelope by $+5''$ in declination (note that declination and zenith angle offsets are approximately equivalent for observations from Hawai‘i of objects which lie at very southern declinations). The outflow velocity in the disk agrees well with the value of $13 \pm 2 \text{ km s}^{-1}$ observed for gas in the dense inner regions as observed in the SiO(6–5) line (Table 1).

5. Discussion

The model shown in Figures 5 and 6, of an expanding disk tilted in the north-south direction, reproduces the observations well, and also agrees with the higher spatial resolution observations of S92, which show that the emission from the envelope is elliptical with the major axis lying east-west. The difference between the discussion by S92 and that here is one of interpretation; S92 suggests that the spatially separated horn features arise from a bipolar flow perpendicular to the disk, while our model identifies them with the northern and southern halves of the tilted disk (cf. Figure 5) whose projected major axis lies east-west. While the fast wind from π^1 Gru is not explicitly modeled, the observations suggest that it is likely to be a continuation of the velocity increase towards the poles.

The model disk which reproduces most of the emission from the inner envelope is much smaller than the envelope extent of $\sim 6 \times 10^{17}$ cm observed via $60 \mu\text{m}$ emission from dust (Young, Phillips and Knapp 1993), and the mass loss rate required to produce the observed emission from the disk is much higher ($1.2 \times 10^{-6} M_\odot \text{ yr}^{-1}$) than the mean value ($\sim 4 \times 10^{-7} M_\odot \text{ yr}^{-1}$) given by the CO line intensity and $60 \mu\text{m}$ flux density. The envelope may thus be roughly spherical, with a strong density increase towards the plane of the disk; alternatively, the mass loss rate of π^1 Gru may have undergone a large increase in the last 1000 years.

The model proposed here for the envelope of π^1 Gru is similar to that suggested for the envelope of the carbon star V Hya by Knapp et al. (1997). The molecular line emission from both envelopes is similar: the lines emitted from the inner envelope have simple parabolic shapes, the CO lines have complex, double horned shapes, and the velocity separation of the horns is significantly smaller than the velocity range of the “high density” emission. Also, both stars have fast ($V_o > 50 \text{ km s}^{-1}$) molecular winds. Fig. 7 reproduces the IRAS color-color diagram for evolved stars with fast molecular winds from Knapp et al. (1997) with the data for π^1 Gru added Jorissen & Knapp (1998); the colors are plotted for the two epochs at which the star was observed. Like V Hya, and unlike all the other stars with fast molecular winds, π^1 Gru still has the infrared colors of an AGB star.

The structure of the π^1 Gru envelope is reminiscent of structure seen in some planetary nebulae. For example, Manchado et al. (1996) have pointed out the existence of a class of quadrupolar planetary nebulae, which they attribute to the presence of two bipolar outflows ejected in different directions. Their proposed model for these flows (see also Livio & Pringle 1996; Guerrero and Manchado 1998) is that the bipolar flow is intermittent and that the flow axis precesses due to the precession of a collimating disk. The similarity of this structure to that suggested from these observations of the π^1 Gru envelope shows that this complex structure is already present in the pre-existing circumstellar envelope. Detailed observa-

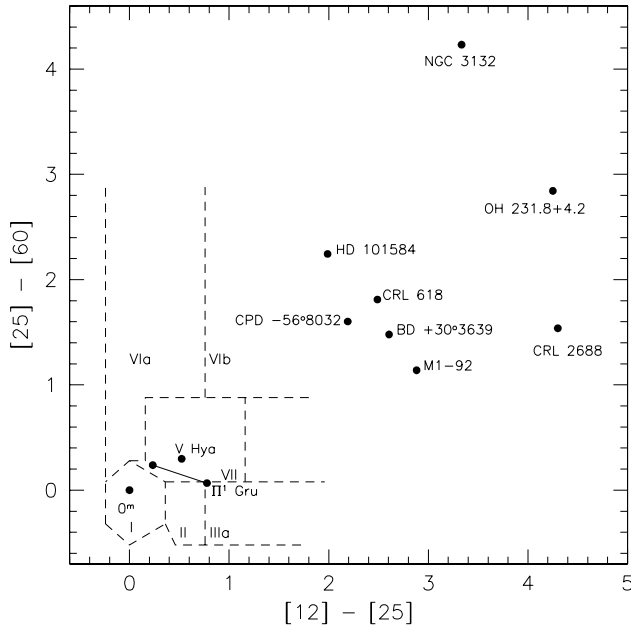


Fig. 7. IRAS color-color diagram for evolved stars with fast molecular winds (cf. Knapp et al. 1997). The dashed lines outline regions I, II, III and VII which are occupied by AGB stars. The two connected points for π^1 Gru correspond to data taken at different epochs (Jorissen & Knapp 1998).

tions of the molecular emission on angular scales of $\leq 1''$ will become possible before too long; it will be interesting to investigate the details of the complex ways in which stars end their lives, which are only dimly discernible in the present observations.

6. Conclusions

1. This paper describes molecular line observations of the envelope around the S star π^1 Gru. We find that the envelope contains complex kinematic structure:
 - (a) A fast molecular wind, with a maximum outflow speed of at least 70 km s^{-1} and perhaps as high as 90 km s^{-1} .
 - (b) A flattened, tilted disk expanding at $15 - 18 \text{ km s}^{-1}$ with a mass loss rate of $1.2 \times 10^{-6} M_{\odot} \text{ yr}^{-1}$ and a kinematic lifetime a factor of 10 smaller than that found for the circumstellar dust distribution.
2. Our model of the molecular line emission from the π^1 Gru envelope shows that the bulk of the emission arises from a disk (and this model also provides a good description of the envelope of the carbon star V Hya). It is of interest that the scale size of the velocity perturbation in the inner envelope (Figure 4) is similar to the projected distance of π^1 Gru's companion, since the separation of the stars is large enough that the companion is expected to have very little effect on a

freely expanding wind (cf. the models of Mastrodemos & Morris 1998; see also Jorissen 1998).

3. The mass loss rate required to produce the flattened disk is several times higher than the mean mass loss rate inferred from the global CO profile or the $60 \mu\text{m}$ emission. The mass loss rate of π^1 Gru may therefore have increased significantly in about the last 1000 years (the kinematic age of the disk). The star may be close to the end of its evolution on the AGB. If so, the present observations show that the production of a fast molecular wind, and of complex envelope structure, begins while the star is still on the AGB.

Acknowledgements. We thank the CSO for providing the observing time for these observations, the staff for their support, and Robert Lupton for help with the plotting program SM. We are grateful to the referee, Garrelt Mellema, for his prompt and very useful report. This research made use of the SIMBAD data base, operated at CDS, Strasbourg, France. Astronomical research at the CSO is supported by the National Science Foundation via grant AST96-15025. Support for this work from Princeton University and from the N.S.F. via grant AST96-18503 is gratefully acknowledged.

References

- Ake, T.B., & Johnson, H.R. 1992, BAAS, 24, 788
 Bernes, C. 1979, A&A, 73, 67
 Crosas, M., & Menten, K. M. 1997, ApJ, 483, 913
 Gezari, D.Y., Schmitz, M., Pitts, P.S., & Mead, J.M. 1993, 'Catalogue of Infrared Observations', NASA RP-1294
 Goldreich, P., & Scoville, N. 1976, ApJ, 205, 144
 Guerrero, M.A., & Machado, A. 1998, ApJ, 508, 262
 Jorissen, A. 1998, in "IAU Symposium 191: AGB Stars" ed. C. Waelkens, D. Reidel Co., in press.
 Jorissen, A., & Knapp, G.R. 1998, A&AS, 129, 363
 Kerschbaum, F., & Hron, J. 1994, A&AS, 106, 397
 Knapp, G.R., Jorissen, A., & Young, K. 1997, A&A, 326, 318
 Kwan, J., & Linke, R.A. 1982, ApJ, 254, 587
 Lambert, D.L., Gustafsson, B., Eriksson, K., & Hinkle, K.H., 1986, ApJS, 62, 373
 Livio, M., & Pringle, J.E. 1996, ApJ, 465, L55
 Lucas, R. 1998, in IAU Symposium 191, Asymptotic Giant Branch Stars, ed. C. Waelkens and T. Le Bertre, in press
 Machado, A., Stanghellini, L., & Guerrero, M. 1996, ApJ, 466, L95
 Mastrodemos, N., & Morris, M. 1998, ApJ, 497, 303
 Monnier, J.D. 1999, in IAU Symposium 191, Asymptotic Giant Branch Stars, ed. C. Waelkens and T. Le Bertre, in press
 Monnier, J.D., Tuthill, P.G., Lopez, B., Cruzalebes, P., Danchi, W.C., & Haniff, C.A. 1999, ApJ (in press: astro-ph/9810024)
 Perryman, M.A.C., Lindegren, L., Kovalevsky, J., et al. 1997, A&A, 323, L49
 Proust, D., Ochsenbein, F., & Petterson, B.R. 1981, A&AS, 44, 179
 Sahai, R. 1992, A&A, 253, L33 (S92)
 Tuthill, P.G., Monnier, J.D., & Danchi, W.C. 1999, in IAU Symposium 191, Asymptotic Giant Branch Stars, ed. C. Waelkens and T. Le Bertre, in press

- van Eck, S., Jorissen, A., Udry, S., Mayor, M., & Pernier, B.
1998, *A&A*, 329, 971
- Young, K., Phillips, T.G., & Knapp, G.R. 1993, *ApJ*, 409, 725